Chemical Physics Letters 674 (2017) 125–129

Contents lists available at ScienceDirect

Chemical Physics Letters

journal homepage: www.elsevier.com/locate/cplett

Research paper

Synthesis and evaluation of α-Ag_2WO_4 as novel antifungal agent

Camila C. Foggi [a], Maria T. Fabbro [b,c], Luís P.S. Santos [d], Yuri V.B. de Santana [e], Carlos E. Vergani [a], Ana L. Machado [a], Eloisa Cordoncillo [f], Juan Andrés [g], Elson Longo [h,*]

[a] Department of Dental Materials and Prosthodontics, Universidade Estadual Paulista, Araraquara 14801-907, Brazil
[b] Department of Chemistry, CDMF, Universidade Federal de São Carlos, 13565-905 São Carlos, Brazil
[c] Instituto Federal de São Paulo, Campus São José dos Campos, Rod. Presidente Dutra km 145, CEP 12223-201, São José dos Campos, SP, Brazil
[d] Department of Chemistry, Instituto Federal do Maranhão, Campus Monte Castelo, 65030-005 São Luís, Brazil
[e] Department of Science, Universidade Tecnológica Federal do Paraná, Campus Cornélio Procópio, 86300-000 Paraná, Brazil
[f] Department of Inorganic and Organic Chemistry, Universitat Jaume I, Campus Riu Sec, E-12071 Castellón, Spain
[g] Department of Physic and Analytical Chemistry, Universitat Jaume I, Campus Riu Sec, E-12071 Castellón, Spain
[h] CDMF, INCTMN, Instituto de Química, Universidade Estadual Paulista, Araraquara 14801-907, Brazil

ARTICLE INFO

Article history:
Received 5 January 2016
In final form 20 February 2017
Available online 22 February 2017

Keywords:
Antifungal activity
α-Ag_2WO_4
Theoretical calculations
Candida albicans

ABSTRACT

Because of the need for new antifungal materials with greater potency, microcrystals of α-Ag_2WO_4, a complex metal oxide, have been synthetized by a simple co-precipitation method, and their antifungal activity against *Candida albicans* has been investigated. A theoretical model based on clusters that are building blocks of α-Ag_2WO_4 has been proposed to explain the experimental results.

1. Introduction

Metal tungstates belong to an important family of inorganic materials that contain a combination of covalent, ionic, and metallic bonds, making them suitable for various technological applications. Among them, silver tungstate (α-Ag_2WO_4), presents a complex three-dimensional structure. At the atomic level, α-Ag_2WO_4 can be described as a network of octahedral [WO_6], pentagonal bipyramid [AgO_7], octahedral [AgO_6], tetrahedral [AgO_4], and angular [AgO_2] clusters, that act as the building blocks of α-Ag_2WO_4, and a weak crystal field is found [1]. α-Ag_2WO_4 has attracted considerable attention in recent years owing to its ability to induce degradation of organic pollutants under UV light irradiation [2], for inducing water splitting to H_2 and O_2 under UV light in the presence of CH_3OH and $AgNO_3$ [3], and for exhibiting visible-light photocatalysis [4–6]. It is also used to produce catalysts [7,8] and light-emitting diodes and gate dielectrics [9]. In addition, it also exhibits photoluminescence activity [10–13].

In a recent study, we evaluated the great potential of α-Ag_2WO_4 nanorod-like structures as novel ozone gas sensors with good sensitivity to low ozone concentrations as well as good stability, fast response, and short recovery time [14], and we analyzed facet-dependent photocatalytic and antibacterial properties in α–Ag_2WO_4 crystals [15]. Further, in many branches of the biomedical field, a current challenge is the synthesis and application of complex metal oxides with enhanced properties with respect to conventional materials. To the best of our knowledge, the antifungal properties of α-Ag_2WO_4 microcrystals have never been evaluated to date. Recently, there has been a dramatic increase in the frequency of systemic fungal infection, and in particular, *Candida albicans* (*CA*) is a major human pathogen that causes local and life-threatening systemic infections [16]. Therefore, the discovery of new antifungal materials with greater potency against *CA* is becoming not only a hot research subject but also a compelling challenge.

In this communication, α-Ag_2WO_4 microcrystals required for this study were synthesized by a simple co-precipitation method. These microcrystals were structurally characterized by X-ray diffraction (XRD), the morphological aspects were investigated by field-emission scanning electron microscopy (FE-SEM) images, and the antifungal action of the microcrystals against *CA* was evaluated.

2. Materials and method

2.1. Synthesis of α-Ag_2WO_4 microcrystals

All the chemicals used were analytical-grade reagents without further purification. Silver tungstate α-Ag_2WO_4 microcrystals were

* Corresponding author.
E-mail address: elson@iq.unesp.br (E. Longo).

http://dx.doi.org/10.1016/j.cplett.2017.02.067
0009-2614/

obtained by the co-precipitation method with polyvinylpyrrolidone (PVP) (Vetec) as surfactant. The synthesis procedure is described as follows: Separately, 1 mmol of sodium tungstate dihydrate ($Na_2WO_2{\cdot}2H_2O$) (99.5% purity, Synth), and 2 mmol of $AgNO_3$ (99.8% purity, Sigma Aldrich) with 0.1 g of PVP were dissolved in 50 mL of deionized water. The two solutions were kept under continuous stirring and heated up to 70 °C. Then, the $AgNO_3$ solution was quickly added to the tungstate solution and the temperature was kept at 70 °C for 10 min. The resultant dark grey precipitates were naturally cooled to room temperature, washed with distilled water and acetone and dried at 60 °C for 24 h.

2.2. Characterization of α-Ag_2WO_4 microcrystals

α-Ag_2WO_4 microcrystals were structurally characterized using XRD patterns obtained using a D/Max-2000PC diffractometer Rigaku (Japan) with Cu Kα radiation (λ = 1.5406 Å) in the 2θ range 10–70° by a scan rate of 2°/min. Morphology (shapes and sizes) of the microcrystals was studied with a FE-SEM model Inspect F50 (FEI Company, Hillsboro, OR), operated at 5 kV.

Photocatalytic selective oxidation of Rhodamine was performed in a 100 mL Pyrex glass bottle under the irradiation of ultraviolet visible light. Controlled photoactivity experiments using different radical scavengers (ammonium oxalate as scavenger for photogenerated holes, $AgNO_3$ as scavenger for electrons, benzoquinone as scavenger for superoxide radical species, and *tert*-butyl alcohol for hydroxyl radical species) were added to the reaction system.

2.3. Antifungal effect of the synthesized α-Ag_2WO_4 microcrystals

To evaluate the antifungal effect of the synthesized microcrystals, the minimum inhibitory concentration (MIC) and the minimum fungicidal concentrations (MFC) for action against planktonic cells were determined using a broth microdilution method as described by Clinical and Laboratory Standards Institute (CLSI), document M27-A3 [17]. MICs were determined as the concentrations of α-Ag_2WO_4 solution at which there was no visible growth, and the MFC values were defined as the lowest concentrations resulting in no growth on plates [18]. A standard strain of *CA* from the American Type Culture Collection (ATCC 90028) was used. To prepare the inoculum, *CA* was streaked onto Sabouraud Dextrose Agar (SDA, Himedia, Mumbai, India) containing 5 μg/mL gentamicin and incubated at 37 °C for 48 h. One loopful of this culture was transferred to 10 ml of RPMI-1640 culture medium (Sigma Chemical, St. Louis, MO) and incubated in an orbital shaker overnight at 37 °C and 75 rpm. Thereafter, *CA* cells were harvested by centrifugation at 4000*g* for 5 min, washed twice with phosphate-buffered saline (PBS, pH 7.2) and resuspended in a RPMI-1640 medium to 10^7 CFU/mL by adjusting the optical density of the suspension to 0.6 at 540 nm.

MIC and MFC were determined by incubating *CA* in 96-well microtiter plates containing 100 μL of the α-Ag_2WO_4 solution (serial 2-fold dilution in RPMI-1640 medium from 1000 to 1.95 μg/mL). Inoculated RPMI-1640 medium, without the microcrystal solutions, was used as positive controls and uninoculated RPMI-1640 medium as negative controls under identical experimental procedures. To establish the MFC values, aliquots from tenfold serial dilution (10^{-1} to 10^{-4}) of each well were inoculated (25 μL) on SDA plates, in duplicates, and incubated for 48 h at 37 °C. Then, the colony-forming units per milliliter (CFU/mL) were calculated and $\log_{10}$ transformed. All experiments were performed independently in triplicate. Since the assumptions of normality and homoscedasticity were found, a parametric one-way ANOVA, followed by multiple pairwise comparisons (*post hoc* Tukey's test), were used to analyze the data (P = 0.05).

FE-SEM was used to observe morphological changes of *C. albicans* when exposed to the silver tungstate microcrystals. For this analysis, *C. albicans* suspensions were inoculated onto polystyrene disks cut to loosely fit in a 24-well microplate (Orange Scientific, Belgium). After 90 min, the medium was aspirated and the non-adherent cells were removed by washing twice with 2 mL of PBS. Ag_2WO_4 microcrystal solution (0.0312 mg/mL) was then added to the wells, and incubated for 24 h at 37 °C. Controls were polystyrene disks inoculated with *C. albicans* for 24 h at 37 °C, without microcrystal solution. Thereafter, the disks were fixed in 4% paraformaldehyde for 4 h at room temperature, dehydrated with a growing ethanol series (70% ethanol for 10 min, 95% ethanol for 10 min and 100% ethanol for 20 min), and dried for 1 h. Then, the disks were mounted onto stubs and sputter coated with gold before analysis.

3. Results and discussion

3.1. X-ray diffraction

Fig. 1 shows the XRD pattern of the as-synthetized α-Ag_2WO_4 and the pure orthorhombic α-Ag_2WO_4 (Inorganic Crystal Structure Database, ICSD, card no. 34-61) indicating that the sample was composed of a single phase only.

3.2. FE-SEM image analyses

The morphology of the sample obtained is shown in Fig. 2. As shown by FE-SEM analysis, the α-Ag_2WO_4 microcrystals has an agglomerate nature and a rod-like elongated shape with length of nearly 1 μm, width of 140 nm and a thickness of approximately 120 nm. The upper right inset is a high magnification FE-SEM image of the sample.

3.3. Antifungal effect of the synthesized α-Ag_2WO_4 microcrystals

A MIC value of 0.0625 mg/mL was obtained for microcrystals. This concentration of α-Ag_2WO_4 microcrystal also inhibited completely the colony growth of *CA* (MFC = 0.0625 mg/mL). The statistical analysis results showed significant effect for the factor concentration (P = 0.0). A significant reduction (P < 0.05) of $\log_{10}$

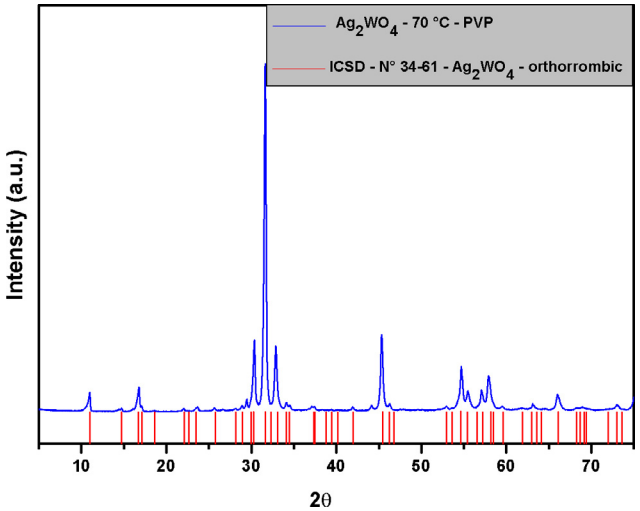

Fig. 1. X-ray pattern for α-Ag_2WO_4 (a) synthesized by co-precipitation method in this work (blue color), and (b) ICSD no. 34–61 (red color). (For interpretation of the references to colour in this figure legend, the reader is referred to the web version of this article.)

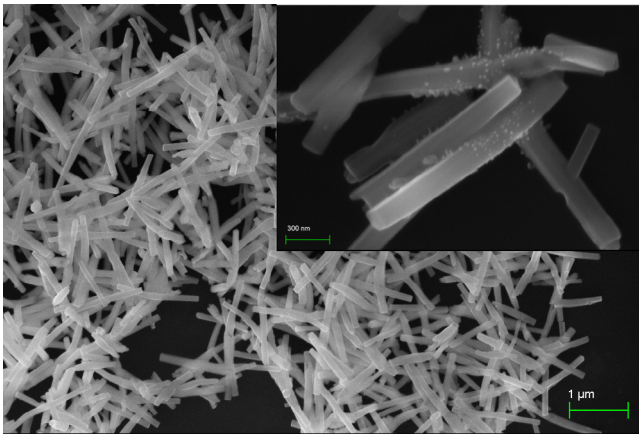

Fig. 2. FE-SEM images of α-Ag_2WO_4 synthesized by co-precipitation with PVP as surfactant. Inset shows the particle morphology with rod-like shape.

CFU/mL values compared to control (from approximately 8 $\log_{10}$ CFU/mL to 5.4 $\log_{10}$ CFU/mL) was observed at concentrations starting at 0.00098 mg/mL.

At the half of MIC/MFC value (0.03125 mg/mL), yeast growth was also significantly reduced to approximately 3 $\log_{10}$ CFU/mL (Fig. 3).

Panáček et al. [19] evaluated the antifungal activity of the silver nanoparticles (NPs) against pathogenic *Candida* spp. For the two clinical strains of *C. albicans*, MIC values were 0.21 mg/L and 0.42 mg/L, showing that the NPs had either comparable or better effects than the tested commercially available antifungal agents (amphotericin B, itraconazole, and fluconazole), with MIC values ranging from ~0.5 mg/L to 1.5 mg/L. It was also found that the NPs killed all of the tested yeasts, but at a higher concentration (MFC = 27 mg/L). More recently, silver nanoparticles were biosynthesized using plant leaf extract and tested for their antifungal activity [20]. The MIC and MFC values of the silver nanoparticles against the same *C. albicans* strain used in the present work (ATCC 90028), were 60 µg/mL and 120 µg/mL, respectively. It is important to emphasize that, while pure silver nanoparticles were evaluated in the cited studies, in the present investigation a compound containing silver (Ag_2WO_4) was used. MIC and MFC values were coincident (0.0625 mg/mL). Based on molecular weight of each component, the amount of silver present on the Ag_2WO_4 microcrystals, at the MIC/MFC concentration, was calculated as being 0.000029 mg/mL. Thus, when Ag_2WO_4 microcrystals are used, the concentrations of silver is dramatically lower as compared to those reported in literature [19,20]. Consequently, Ag_2WO_4 microcrystals presented here have far lower propensity to induce cytotoxic effect to mammalian cells [21].

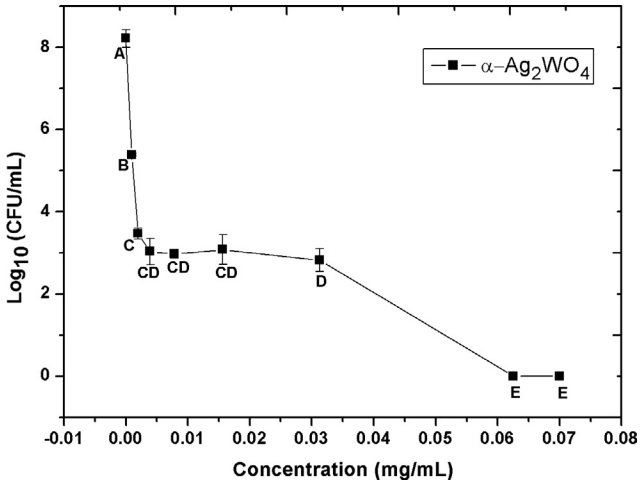

Fig. 3. Summary of $\log_{10}$ CFU/mL values obtained for the concentrations of the α-Ag_2WO_4. Different capital letters denote significant difference ($P < 0.05$) according to the *post hoc* test.

As mentioned above, α-Ag_2WO_4 is formed by octahedral [WO_6], pentagonal bipyramid [AgO_7], octahedral [AgO_6], tetrahedral [AgO_4], and angular [AgO_2] clusters. In this structure, the Ag-O and W-O bonds, and O-Ag-O and O-W-O bond angles are free to stretch/shorten and bend, respectively, resulting in the variation of bond lengths and angles, as well the rotations of the [AgO_y] (y = 2, 4, 6, and 7) and [WO_6] clusters, which are responsible for the electronic structure of Ag_2WO_4 phases. Therefore, an important impact on crystal field can be sensed as well as in the dipoles and electronic band structures, thereby influencing the behaviors of photogenerated charge carriers, including excitation, transfer, and redox reaction, in whole photocatalytic process [4,10,22]. This is due to the fact that the clusters rotations influence the Ag-O and W-O bond lengths as well as the Ag-O-Ag and W-O-W bond angles due to the shift of the oxygen ions from the edges of the ideal structures. Subsequently, the relative positions of O, W, and Ag atoms are variable.

Based on this behavior, our model for α-Ag_2WO_4 crystals is composed of by different types of distorted clusters ([WO_6]$_d$, [AgO_7]$_d$, [AgO_6]$_d$, [AgO_4]$_d$, and [AgO_2]$_d$) and ordered clusters ([WO_6]$_o$, [AgO_7]$_o$, [AgO_6]$_o$, [AgO_4]$_o$, and [AgO_2]$_o$) [23]. α-Ag_2WO_4 is a semiconductor with a band gap of about 3.1 eV, so it cannot be activated by visible light. Therefore, other characteristic is also very important for improve the activity, such as intrinsic defects in the lattice that are capable to produce intermediary levels between the valence band and the conduction band. These structural defects, which are caused by distorted [WO_6]$_d$/[AgO_y]$_d$ (y = 2, 4, 6, and 7) clusters, can polarize the lattice and lead to electronic transitions between disordered $[WO_6]_d^x/[AgO_y]_d^x$ and ordered $[WO_6]_o^x/[AgO_y]_o^x$ clusters. Interestingly, different morphologies will have different exposed facets which in turn modulate the antifungal behavior of the material [15]. In our case, the exposed faces of α-Ag_2WO_4 are (010), (100), (001), (101), (110) and (011), and it is important to note that the (001) and (101) exposed faces are O- and Ag-terminated and they are the most stable surfaces of α-Ag_2WO_4 [24]. The highest activity of (001) and (101) surfaces can be attributed to the overall arrangement of Ag atoms in these planes and the sub-layer, which could probably result in favorable electronic interactions, creating a site for substrate binding for O_2 and H_2O and the subsequent formation of reactive radicals [15]. Based on these assumptions, the following processes can occur in α-Ag_2WO_4 crystals, as expressed by the Eqs. (1)(8).

$$[AgO_y]_o^x + [AgO_y]_d^x \rightarrow [AgO_y]_o' - [AgO_y]_d^{\cdot} \quad (1)$$

where y = 2, 4, 6 and 7.

$$[WO_6]_o^x + [WO_6]_d^x \rightarrow [WO_6]_o' + [WO_6]_d^{\cdot} \quad (2)$$

$$[WO_6]_o' + [WO_6]_d^{\cdot} + O_2 \rightarrow [WO_6]_o^x + [WO_6]_d^{\cdot} \ldots O_{2(ads)}' \quad (3)$$

$$[WO_6]_o' + [WO_6]_d^{\cdot} + H_2O \rightarrow [WO_6]_o^x + [WO_6]_d^{\cdot} \ldots OH_{(ads)}^{*} + H^{\cdot} \quad (4)$$

$$[WO_6]_o^x + [WO_6]_d^{\cdot} \ldots O_{2(ads)}' + H^{\cdot} \rightarrow [WO_6]_o^x + [WO_6]_d^{\cdot} + O_2H^{*} \quad (5)$$

$$[AgO_y]_o' + [AgO_y]_d^{\cdot} + O_2 \rightarrow [AgO_y]_o^x + [AgO_y]_d^{\cdot} \ldots O_{2(ads)}' \quad (6)$$

$$[AgO_y]_o' + [AgO_y]_d^{\cdot} + H_2O \rightarrow [AgO_y]_o' + [AgO_y]_d^x \ldots OH_{(ads)}^{*} + H^{\cdot} \quad (7)$$

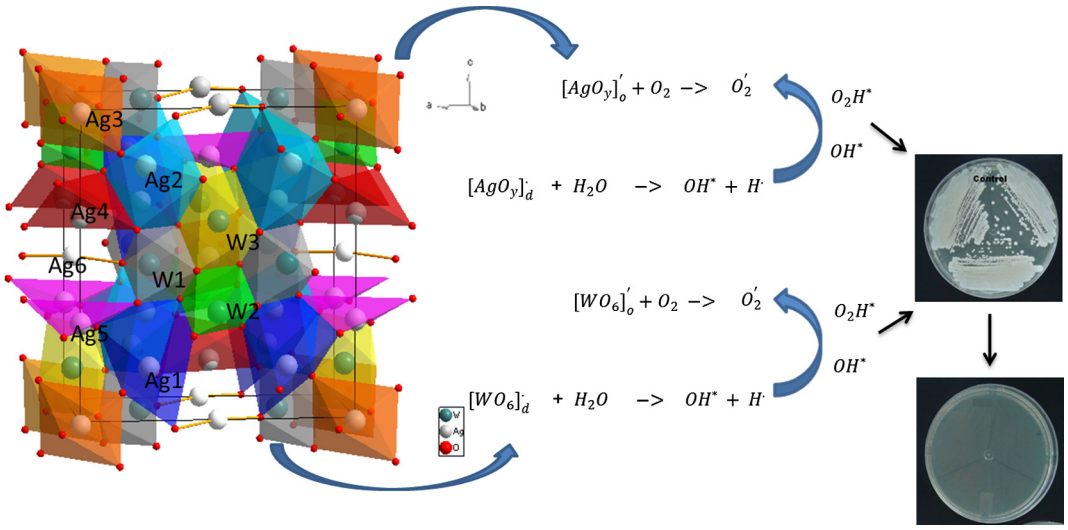

Fig. 4. A Schematic proposal for the mechanism of action of α-Ag_2WO_4. The octahedral [WO_6] (in grey, green and yellow), pentagonal bipyramid [AgO_7] (in blue), octahedral [AgO_6] (in golden), tetrahedral [AgO_4] (in red), and angular [AgO_2] clusters, as constituents building blocks of α-Ag_2WO_4 are depicted. (For interpretation of the references to colour in this figure legend, the reader is referred to the web version of this article.)

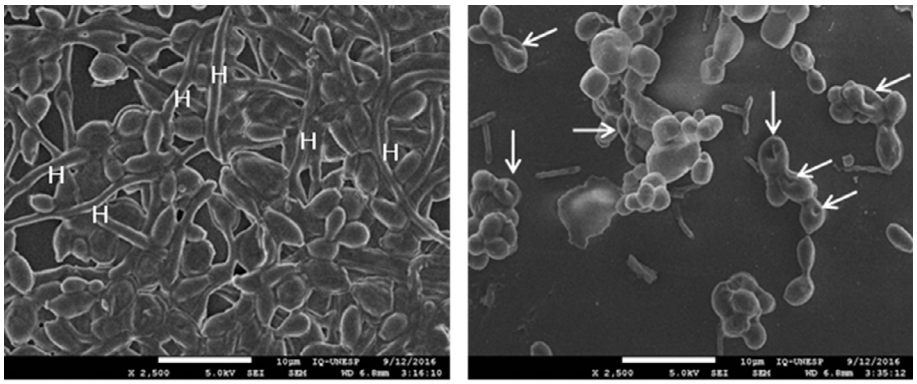

Fig. 5. FE-SEM of *C. albicans* cells incubated without (a) and with the Ag_2WO_4 microcrystals (b). H: hyphae. White arrows: morphological changes of *C. albicans* cells.

$$[AgO_y]^x_o + [AgO_y]^{\cdot}_d \ldots O'_{2(ads)} + H^{\cdot} \rightarrow [AgO_y]^x_o + [AgO_y]^{\cdot}_d + O_2H^* \quad (8)$$

In these equations, the superscript *x* indicates neutral clusters, (′) the cluster with one electron, (•) the cluster with one hole, and (∗) reactive radicals. Thus, we assume that the defects on the crystal surface with presence of under coordinated Ag atoms with respect to the ideal (ordered) cluster as well as the electronic structure of these disordered $[WO_6]^{\cdot}_d$ and $[AgO_y]^{\cdot}_d$ and ordered $[WO_6]'_o$ and $[AgO_y]'_o$ clusters play an important role in the production of OH^* and O_2H^* radicals, which are the most oxidizing species in these chemical reactions that kill *CA*. Fig. 4 shows a pictorial representation of our proposed model.

The photocatalytic procedure shows that semiconductor interaction with water and oxygen results in high concentration of the peroxide radical relative to the hydroxyl radical bactericidal activity.

FE-SEM images show that the untreated *C. albicans* cells (control) preserved their normal morphology (Fig. 5a), with cell aggregates and presence of hyphal cells. In contrast, *C. albicans* cells exposed to the Ag_2WO_4 microcrystals showed irregular surface and shriveled appearance, with absence of hyphae cells. It is known that *C. albicans* can switch morphology from yeast to pseudohyphal or hyphal form [25]. This ability to switch between morphologies is often considered a major virulence factor, since hyphal cells are responsible for infection in the host and are able to invade tissues [18].

4. Conclusions

α-Ag_2WO_4 microcrystals were successfully obtained by using a rapid, cost-effective method, namely, the co-precipitation method. We described a systematic investigation on the antifungal activity of α-Ag_2WO_4 against *CA*. The as-synthesized microcrystals were capable of inactivating and killing the *CA* cells at a concentration of 0.0625 mg/mL. Moreover, exposure to sub-inhibitory concentrations of the microcrystals yielded a reduction in the number of viable cells by more than 5 $\log_{10}$ CFU/mL, demonstrating that α-Ag_2WO_4 has great potential as an antifungal agent. Reactive oxygen species (ROS) apparently played a major role in cell death. The electronic properties of α-Ag_2WO_4 are to be strongly dependent on the distortions of the crystal lattice, such as Ag-O and W-O bond distances, and O-Ag-O and O-W-O bond angles, and deformations of the [WO_6] and [AgO_y] (y = 2, 4, 6 and 7) clusters,

as building blocks of α-Ag_2WO_4. A theoretical model based on the distortions of these clusters has been proposed to explain the experimental results; this model denotes a shift in the conceptualization of the role of α-Ag_2WO_4 microcrystals in biological systems, indicating that the crystal structure plays an important role. We believe that the results presented herein offer new insights regarding the various parameters that dictate the antifungal activity of α-Ag_2WO_4. In future, the possibility of a broad spectrum of interactions between these complex metal oxides and antifungal systems can be explored.

Acknowledgement

The authors acknowledge the financial support of the following agencies: Conselho Nacional de Desenvolvimento Científico e Tecnológico: 237944/2012-0; Fundação de Amparo à Pesquisa do Estado de São Paulo: 2015/03654-7; Generalitat Valenciana for *PrometeoII*/2014/022 and ACOMP/2014/270, Ministerio de Economia y Competitividad, project CTQ2012-36253-C03-02., Programa de Cooperación Científica con Iberoamerica (Brasil), Ministerio de Educación (PHB2009-0065-PC). J.A. acknowledges to Ministerio de Economia y Competitividad, 'Salvador Madariaga' program, PRX15/00261.

References

[1] C. Janáky, K. Rajeshwar, N.R. de Tacconi, W. Chanmanee, M.N. Huda, Tungsten-based oxide semiconductors for solar hydrogen generation, Catal. Today 199 (2013) 53–64, http://dx.doi.org/10.1016/j.cattod.2012.07.020.
[2] H. Chen, Y. Xu, Photoactivity and stability of Ag_2WO_4 for organic degradation in aqueous suspensions, Appl. Surf. Sci. 319 (2014) 319–323, http://dx.doi.org/10.1016/j.apsusc.2014.05.115.
[3] J. Tang, J. Ye, Correlation of crystal structures and electronic structures and photocatalytic properties of the W-containing oxides, J. Mater. Chem. 15 (2005) 4246, http://dx.doi.org/10.1039/b504818d.
[4] Z. Lin, J. Li, Z. Zheng, J. Yan, P. Liu, C. Wang, G. Yang, Electronic reconstruction of α-Ag_2WO_4 nanorods for visible-light photocatalysis, ACS Nano 9 (2015) 7256–7265, http://dx.doi.org/10.1021/acsnano.5b02077.
[5] A. Thomas, C. Janáky, G.F. Samu, M.N. Huda, P. Sarker, J.P. Liu, V. van Nguyen, E. H. Wang, K.A. Schug, K. Rajeshwar, Time- and energy-efficient solution combustion synthesis of binary metal tungstate nanoparticles with enhanced photocatalytic activity, ChemSusChem 8 (2015) 1652–1663, http://dx.doi.org/10.1002/cssc.201500383.
[6] D. Xu, B. Cheng, J. Zhang, W. Wang, J. Yu, W. Ho, Photocatalytic activity of Ag_2MO_4 (M = Cr, Mo, W) photocatalysts, J. Mater. Chem. A 3 (2015) 20153–20166, http://dx.doi.org/10.1039/C5TA05248C.
[7] C.-X. Guo, B. Yu, J.-N. Xie, L.-N. He, Silver tungstate: a single-component bifunctional catalyst for carboxylation of terminal alkynes with CO_2 in ambient conditions, Green Chem. 17 (2015) 474–479, http://dx.doi.org/10.1039/C4GC01638F.
[8] J. Andrés, L. Gracia, P. Gonzalez-Navarrete, V.M. Longo, W. Avansi, D.P. Volanti, M.M. Ferrer, P.S. Lemos, F.A. La Porta, A.C. Hernandes, E. Longo, Structural and electronic analysis of the atomic scale nucleation of Ag on α-Ag_2WO_4 induced by electron irradiation, Sci. Rep. 4 (2014) 5391, http://dx.doi.org/10.1038/srep05391.
[9] A. Sreedevi, K.P. Priyanka, S.R. Mary, E.M. Mohammed, T. Varghese, Nanophase α-silver tungstate for potential applications in light emitting diodes and gate dielectrics, Adv. Sci. Eng. Med. 7 (2015) 498–505, http://dx.doi.org/10.1166/asem.2015.1712.
[10] L.S. Cavalcante, M.A.P. Almeida, W. Avansi, R.L. Tranquilin, E. Longo, N.C. Batista, V.R. Mastelaro, M.S. Li, Cluster coordination and photoluminescence properties of α-Ag_2WO_4 microcrystals, Inorg. Chem. 51 (2012) 10675–10687, http://dx.doi.org/10.1021/ic300948n.
[11] E. Longo, D.P. Volanti, V.M. Longo, L. Gracia, I.C. Nogueira, M.A.P. Almeida, A.N. Pinheiro, M.M. Ferrer, L.S. Cavalcante, J. Andrés, Toward an understanding of the growth of Ag filaments on α-Ag_2WO_4 and their photoluminescent properties: a combined experimental and theoretical study, J. Phys. Chem. C 118 (2014) 1229–1239, http://dx.doi.org/10.1021/jp408167v.
[12] E. Longo, L.S. Cavalcante, D.P. Volanti, A.F. Gouveia, V.M. Longo, J.A. Varela, M. O. Orlandi, J. Andrés, Direct in situ observation of the electron-driven synthesis of Ag filaments on α-Ag_2WO_4 crystals, Sci. Rep. 3 (2013) 1676, http://dx.doi.org/10.1038/srep01676.
[13] Y.V.B. De Santana, J.E.C. Gomes, L. Matos, G.H. Cruvinel, A. Perrin, C. Perrin, J. Andres, J.A. Varela, E. Longo, Silver molybdate and silver tungstate nanocomposites with enhanced photoluminescence, Nanomater. Nanotechnol. 4 (2014) 1, http://dx.doi.org/10.5772/58923.
[14] L.F. da Silva, A.C. Catto, W. Avansi, L.S. Cavalcante, J. Andrés, K. Aguir, V.R. Mastelaro, E. Longo, A novel ozone gas sensor based on one-dimensional (1D) α-Ag_2WO_4 nanostructures, Nanoscale 6 (2014) 4058–4062, http://dx.doi.org/10.1039/c3nr05837a.
[15] R.A. Roca, J.C. Sczancoski, I.C. Nogueira, M.T. Fabbro, H.C. Alves, L. Gracia, L.P.S. Santos, C.P. de Sousa, J. Andrés, G.E. Luz, E. Longo, L.S. Cavalcante, Facet-dependent photocatalytic and antibacterial properties of α-Ag_2WO_4 crystals: combining experimental data and theoretical insights, Catal. Sci. Technol. 5 (2015) 4091–4107, http://dx.doi.org/10.1039/C5CY00331H.
[16] A.M. Qandil, M.A. Hassan, N.A. Al-Shar'i, Synthesis and anticandidal activity of azole-containing sulfonamides, Arch. Pharm. (Weinheim) 341 (2008) 99–112, http://dx.doi.org/10.1002/ardp.200700125.
[17] CLSI, Reference Method for Broth Dilution Antifungal Susceptibility Testing of Yeasts; Approved Standard, third ed., Clinical and Laboratory Standards Institute, Wayne, PA, 2008.
[18] C.A. Zamperini, R.S. André, V.M. Longo, E.G. Mima, C.E. Vergani, A.L. Machado, J. A. Varela, E. Longo, Antifungal applications of Ag-decorated hydroxyapatite nanoparticles, B3 – J. Nanomater. 2013 (2013) 1–9, http://dx.doi.org/10.1155/2013/174398.
[19] A. Panáček, M. Kolář, R. Večeřová, R. Prucek, J. Soukupová, V. Kryštof, P. Hamal, R. Zbořil, L. Kvítek, Antifungal activity of silver nanoparticles against Candida spp, Biomaterials 30 (2009) 6333–6340, http://dx.doi.org/10.1016/j.biomaterials.2009.07.065.
[20] N. Khatoon, A. Mishra, H. Alam, N. Manzoor, M. Sardar, Biosynthesis, characterization, and antifungal activity of the silver nanoparticles against pathogenic candida species, Bionanoscience 5 (2015) 65–74, http://dx.doi.org/10.1007/s12668-015-0163-z.
[21] A. Panáček, M. Smékalová, R. Večeřová, K. Bogdanová, M. Röderová, M. Kolář, M. Kilianová, Š. Hradilová, J.P. Froning, M. Havrdová, R. Prucek, R. Zbořil, L. Kvítek, Silver nanoparticles strongly enhance and restore bactericidal activity of inactive antibiotics against multiresistant Enterobacteriaceae, Colloids Surf. B Biointerf. 142 (2016) 392–399, http://dx.doi.org/10.1016/j.colsurfb.2016.03.007.
[22] J. Andrés, L. Gracia, P. Gonzalez-Navarrete, V.M. Longo, W. Avansi, D.P. Volanti, M.M. Ferrer, P.S. Lemos, F.A. La Porta, A.C. Hernandes, E. Longo, Structural and electronic analysis of the atomic scale nucleation of Ag on α-Ag_2WO_4 induced by electron irradiation, Sci. Rep. 4 (2014) 5391, http://dx.doi.org/10.1038/srep05391.
[23] V.M. Longo, C.C. De Foggi, M.M. Ferrer, A.F. Gouveia, R.S. André, W. Avansi, C.E. Vergani, A.L. Machado, J. Andrés, L.S. Cavalcante, A.C. Hernandes, E. Longo, Potentiated electron transference in α-Ag_2WO_4 microcrystals with Ag nanofilaments as microbial agent, J. Phys. Chem. A 118 (2014) 5769–5778, http://dx.doi.org/10.1021/jp410564p.
[24] J. Andrés, L. Gracia, A.F. Gouveia, M.M. Ferrer, E. Longo, Effects of surface stability on the morphological transformation of metals and metal oxides as investigated by first-principles calculations, Nanotechnology 26 (2015) 405703, http://dx.doi.org/10.1088/0957-4484/26/40/405703.
[25] S.W. Kim, Y.J. Joo, J. Kim, Asc1p, a ribosomal protein, plays a pivotal role in cellular adhesion and virulence in Candida albicans, J. Microbiol. 48 (2010) 842–848, http://dx.doi.org/10.1007/s12275-010-0422-1.